2-1-2012

Epithelial Na $^{+}$ sodium channels in magnocellular cells of the rat supraoptic and paraventricular nuclei

Ryoichi Teruyama
Louisiana State University

Mayumi Sakuraba
University of Tennessee Health Science Center

Lori L. Wilson
Louisiana State University

Narine E.J. Wandrey
Louisiana State University

William E. Armstrong
University of Tennessee Health Science Center

Recommended Citation

Teruyama, R., Sakuraba, M., Wilson, L., Wandrey, N., & Armstrong, W. (2012). Epithelial Na $^{+}$ sodium channels in magnocellular cells of the rat supraoptic and paraventricular nuclei. *American Journal of Physiology - Endocrinology and Metabolism, 302* (3), 273-285. https://doi.org/10.1152/ajpendo.00407.2011

Am J Physiol Endocrinol Metab 302: E273–E285, 2012.
First published November 1, 2011; doi:10.1152/ajpendo.00407.2011.

Epithelial Na^+ sodium channels in magnocellular cells of the rat supraoptic and paraventricular nuclei

Ryoichi Teruyama,[1] Mayumi Sakuraba,[2] Lori L. Wilson,[1] Narine E. J. Wandrey,[1] and William E. Armstrong[2]

[1]*Department of Biological Sciences, Louisiana State University, Baton Rouge, Louisiana; and* [2]*Department of Anatomy and Neurobiology, University of Tennessee Health Science Center, Memphis, Tennessee*

Submitted 5 August 2011; accepted in final form 31 October 2011

Teruyama R, Sakuraba M, Wilson LL, Wandrey NE, Armstrong WE. Epithelial Na^+ sodium channels in magnocellular cells of the rat supraoptic and paraventricular nuclei. *Am J Physiol Endocrinol Metab* 302: E273–E285, 2012. First published November 1, 2011; doi:10.1152/ajpendo.00407.2011.—The epithelial Na^+ channels (ENaCs) are present in kidney and contribute to Na^+ and water homeostasis. All three ENaC subunits (α, β, and γ) were demonstrated in the cardiovascular regulatory centers of the rat brain, including the magnocellular neurons (MNCs) in the supraoptic nucleus (SON) and the paraventricular nucleus (PVN). However, the functional significance of ENaCs in vasopressin (VP) and oxytocin (OT) synthesizing MNCs is completely unknown. In this study, we show with immunocytochemical double-labeling that the α-ENaC is colocalized with either VP or OT in MNCs in the SON and PVN. In addition, parvocellular neurons in the dorsal, ventrolateral, and posterior subregions of the PVN (not immunoreactive to VP or OT) are also immunoreactive for α-ENaC. In contrast, immunoreactivity to β- and γ-ENaC is colocalized with VP alone within the MNCs. Furthermore, immunoreactivity for a known target for ENaC expression, the mineralcorticoid receptor (MR), is colocalized with both VP and OT in MNCs. Using single-cell RT-PCR, we detected mRNA for all three ENaC subunits and MR in cDNA libraries derived from single MNCs. In whole cell voltage clamp recordings, application of the ENaC blocker benzamil reversibly reduced a steady-state inward current and decreased cell membrane conductance approximately twofold. Finally, benzamil caused membrane hyperpolarization in a majority of VP and about one-half of OT neurons in both spontaneously firing and quiet cells. These results strongly suggest the presence of functional ENaCs that may affect the firing patterns of MNCs, which ultimately control the secretion of VP and OT.

aldodsterone; vasopressin; oxytocin

THE NEUROHYPOPHYSIAL HORMONES vasopressin (VP) and oxytocin (OT) are synthesized in the magnocellular neurons (MNCs) located within the paraventricular nucleus (PVN) and the supraoptic nucleus (SON) of the hypothalamus and released from the neurohypophysis into the general circulation in response to physiological demands. The secretion of VP increases in response to hyperosmolality, hypovolemia, and hypotension and produces antidiuretic and pressor effects (59). In addition to the well-known effects of OT during parturition and lactation, plasma OT also increases with hyperosmolality and hypernatremia (32) and induces natriuresis (13, 31).

The non-voltage-dependent, amiloride-sensitive epithelial Na^+ channels (ENaCs) are present in the apical membrane of epithelial cells in a variety of tissues, such as urinary bladder, renal collecting duct, distal colon, sweat and salivary glands, lung, and taste buds, and are known to mediate the transport of Na^+ across epithelia (7, 21). Thus, together with the Na^+/K^+-ATPase present in the basal membrane of epithelial cells, ENaCs regulate transepithelial Na^+ transport; however, entry across the apical membrane through ENaCs is the rate-limiting step under most circumstances (21). The ENaCs located in the distal nephron in kidney are known to finely regulate blood pressure and extracellular fluid volume by modulating Na^+ excretion and reabsorption (7, 21). Activity of ENaCs is regulated largely by the adrenal mineralocorticoid aldosterone through its mineralocorticoid receptor (MR) (42).

Interestingly, both mRNA and protein for all three ENaC subunits (α, β, and γ) and MR were demonstrated in regions implicated in cardiovascular control, such as the MNCs in the SON and PVN, and also in the hippocampus, choroid plexus, ependyma, and brain blood vessels in rats (4). The physiological function of the ENaC in neurons is not well understood; however, the locations of ENaC in the brain suggest a role in cardiovascular regulation. Intracerebroventricular (icv) infusion of aldosterone increases blood pressure, presumably via upregulation of ENaC in the brain in Wistar rats (68, 69) and in an animal model of salt-sensitive hypertension, Dahl salt-sensitive (Dahl-S) rats (25). Importantly, icv injections of the ENaC blocker, the amiloride analog benzamil, significantly attenuated hypertension in these animals (27, 47). These findings suggest that aldosterone-mediated activation of ENaCs in brain could contribute to the development of hypertension and that central ENaC inhibition may be a potential new target in the treatment of cardiovascular disease (63). However, the significance of ENaCs in regulating MNC electrical activity is unknown. In the present study, we confirmed the presence of ENaCs and MR in MNCs and determined the extent of their selective expression in VP and OT neurons, and for the first time we show that ENaCs contribute to the membrane potential in these neurons.

MATERIALS AND METHODS

Animals

Male Sprague-Dawley rats were used (180–210 g body wt; Harlan Laboratories, Indianapolis, IN). The rats were housed in a room on a 12:12-h light-dark cycle, with access to food and water available ad libitum. All protocols were approved by the Institutional Animal Care and Use Committees at the University of Tennessee and Louisiana State University.

Electrophysiology

Slice preparation. The rats were deeply anesthetized with pentobarbital sodium (50 mg/kg ip) and perfused through the heart with

Address for reprint requests and other correspondence: R. Teruyama, Louisiana State University, 202 Life Sciences Bldg., Baton Rouge, LA 70803 (e-mail: rteruyama@lsu.edu).

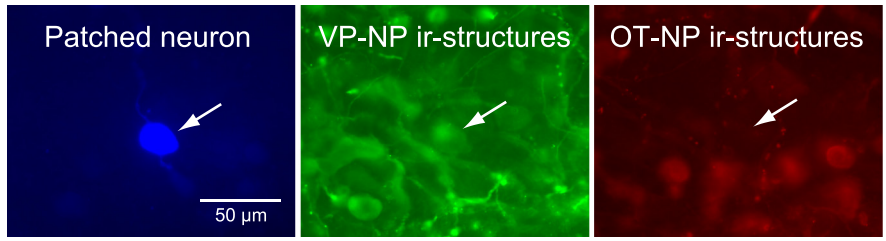

Fig. 1. Immunocytochemical identification of cell types in the recorded magnocellular neuron (MNC). The patched neurons were filled with biocytin and visualized by 7-amino-4-methylcoumarin-3-acetic acid (AMCA)-conjugated avidin (*left* arrow). The tissue was also labeled for vasopressin (VP)- and oxytocin (OT)-neurophysins (NP) by immunofluorescence using DyLight 488- and DyLight 594-conjugated secondary antibodies, respectively. The recorded cell (*left* arrow) was immunoreactive (ir) to VP-NP (*middle* arrow) but not to OT-NP (*right* arrow).

cold artificial cerebrospinal fluid (ACSF; see below), in which NaCl was replaced by an equiosmolar amount of sucrose. Brains were removed, and coronal slices (250 μm) containing SON were obtained by a vibrating blade microtome (Leica VT1000S; Leica, Mannheim, Germany).

Recording. Whole cell patch clamp recordings were acquired digitally at 20 kHz and filtered at 5 kHz with a Digidata 1440A and an Axopatch 700A or 700B (Molecular Devices, Foster City, CA) amplifier in conjunction with PClamp 10 software (Molecular Devices) on a Windows platform PC. The MNCs in the SON were identified visually using an Olympus BX50WI microscope and a ×40 water immersion lens (0.8 na) under IR illumination (780 ± 30 nm) using a charge-coupled device camera. Recordings were taken using borosilicate electrodes (4–8 MΩ resistance) produced with a horizontal electrode puller (Model P-87 Flaming/Brown Micropipette puller; Sutter Instruments, Novato, CA). The patch solution for voltage clamp experiment contained (in mM) 100 D-gluconic acid, 100 CsOH, 20 CsCl, 10 HEPES, 11 EGTA, 1 CaCl2, 2 MgCl2, 10 NaCl, 2 adenosine 5′-triphosphate (ATP), and 0.4 guanosine 5′-triphosphate (GTP) and for current clamp experiment contained (in mM) 140 K-gluconate, 1 $MgCl_2$, 10 HEPES, 1 $CaCl_2$, 2 ATP (Mg^{++}), 0.4 GTP (Na^+), and 1 EGTA. The patch solutions also contained 0.2% biocytin (Sigma) to fill the patched cell (64, 65). The ACSF consisted of (in mM) 125 NaCl, 2.5 KCl, 1 $MgSO_4$, 1.25 NaH_2PO_4, 26 $NaHCO_3$, 20 D-glucose, 2 $CaCl_2$, and 0.4 ascorbic acid. The medium was saturated with 95% O_2-5% CO_2, with a pH of 7.3–7.4 and an osmolality of 290–300 mOsm/kg H_2O. Picrotoxin and DNQX (100 and 10 μM, respectively) were also added to ACSF to suppress the synaptic activity. Solutions were warmed to 33–34°C during the recordings.

Post Hoc Immunocytochemical Identification of Cell Types

The slices were fixed (4% paraformaldehyde-0.1% picric acid in 0.15 M sodium phosphate buffer, pH 7.2–7.4) and processed for double-immunofluorescence labeling to identify the cell type (64, 65). To identify VP neurons, a specific VP-neurophysin (NP) polyclonal antibody (53) raised in rabbits was used at a 1:20,000 dilution [provided by Alan Robinson, University of California Los Angeles (UCLA)]. For OT neurons, a specific anti-OT-NP monoclonal antibody (6) raised in mouse is used at a 1:500 dilution (PS38; provided by Harold Gainer, National Institutes of Health). Slices were incubated for 48–72 h at 4°C, followed by the incubation in a cocktail of secondary antibodies and avidin-AMCA (7-amino-4-methylcoumarin-3-acetic acid; Vector Laboratories, Burlingame, CA), overnight at 4°C. The secondary antibodies were Alexa Fluor 488-conjugated goat anti-rabbit and Alexa Fluor 568-conjugated goat anti-mouse IgG (Invitrogen, Eugene, OR). Avidin-AMCA was used to visualize biocytin-filled neurons. Neurons were considered as either OT or VP types only if positive staining of one antibody was complemented by a negative reaction for the other one (Fig. 1).

Double Immunolabeling

The antibodies against α-, β-, and γ-ENaC subunits (3560-2, 3755-2, and 550, respectively) were raised in rabbit and were a kind gift from Dr. Mark A. Knepper (National Institutes of Health, Bethesda, MD). The production and characterization of these ENaC subunit antibodies were described previously in great detail (42). The anti-VP-NP (PS41) and the anti-OT-NP (PS38) were raised in mouse against VP-NP or OT-NP, respectively (6), and used at a 1:500 dilution (see above). The slices were first incubated with one of the anti-ENaC subunits for 48–72 h at 4°C, followed by the incubation with either anti-VP-NP or anti-OT-NP for 48–72 h at 4°C.

The monoclonal anti-mineralocorticoid receptor antibody (MRN3 3F10) developed by C. E. Gomez-Sanchez was obtained from the Developmental Studies Hybridoma Bank developed under the auspices of the National Institute of Child Health and Human Development and maintained by The University of Iowa, Department of Biology, Iowa City, IA. The production and characterization of the MR antibody were described previously in great detail (24). The anti-VP-NP (Rob-VP) and the anti-OT-NP (Rob-OT) antiserum used for double labeling with MR antibody were provided by Alan Robinson (UCLA). Rob-VP and -OT antisera (53) were raised in rabbit against VP-NP or OT-NP, respectively, and used at 1:20,000 and 1:10,000 dilutions, respectively.

After incubations with primary antibodies, the slices were incubated in a cocktail of appropriate secondary antibodies for 2 h at room temperature. The secondary antibodies used were DyLight 488-conjugated goat anti-rabbit and DyLight 594-conjugated goat anti-mouse IgG (Jackson ImmunoResearch, West Grove, PA). The brain slices were examined, and confocal images (1,024 × 1,024) were acquired with a confocal microscope (Leica TCS SP2 spectral confocal microscope). The optical section thickness was 1 μm. These were viewed in stacks of three to five sections using ImageJ software (NIH).

Table 1. *Primer sequences used to detect gene expressions of interest*

Gene	Primer Sequence	Amplicon Size, bp
α-ENaC		
Forward	5′-GTTCTGTGACTACCGAAAGCAGAG-3′	429
Reverse	5′-CGTAGCAGCATGAGAAGTGTGATG-3	
β-ENaC		
Forward	5′-ACCCTGAGCAGGAAGGGTAT-3′	220
Reverse	5′-ACAGGAGGCCACTAGCTTGA-3	
γ-ENaC		
Forward	5′-CGTCAGTGGCACAAAGCCAA-3′	301
Reverse	5′-GAGAGCCTCCTCAAACCATG-3′	
MR		
Forward	5′-GCTCAACATTGTCCAGTACA-3′	260
Reverse	5′-GCACAGGTGGTCCTAAGATT-3′	
OT		
Forward	5′-GACGGTGGATCTCGGACTGAA-3′	463
Reverse	5′-CGCCCCTAAAGGTATCATCACAAA-3′	
VP		
Forward	5′-CCTCACCTCTGCCTGCTACTT-3′	440
Reverse	5′-GGGGGCGATGGCTCAGTAGAC-3′	

ENaC, epithelial Na^+ channel; MR, mineralocorticoid receptor; OT, oxytocin; VP, vasopressin.

Single-Cell RT-PCR

Single-cell harvest for single-cell RT-PCR. The brains were sliced as described in *Slice preparation*. Small pieces of brain (~2 × 2 mm) containing the SON were dissected from the slices under a stereomicroscope. These pieces were incubated in oxygenated ACSF (35°C) containing protease type XIV (1.2 mg/ml; Sigma Chemical, St. Louis, MO) for 20–30 min and then washed with sodium isethionate solution (in mM: 140 sodium isethionate, 2 KCl, 4 $MgCl_2$, 23 glucose, 15 HEPES, pH 7.3). The enzyme-treated tissues were triturated in sodium isethionate solution using three successively smaller fire-polished pipettes to release individual MNC cell bodies. The supernatant containing dissociated neurons from each trituration step was transferred to a plastic Petri dish (Nunc, Rochester, NY) on an inverted microscope stage, and cells were allowed to settle for ~5 min. A background flow of ~1 ml/min of HEPES-buffered saline solution (HBSS) was then established. HBSS consisted of (in mM) 138 NaCl, 3 KCl, 1 $MgCl_2$, 2 $CaCl_2$, 10 HEPES, and 20 dextrose, pH 7.3 (adjusted with 1 N NaOH), and osmolarity = 300–305 mOsmol/l.

Electrode glass (Corning 7052 capillary glass; Garner Glass, Claremont, CA) was autoclaved to prevent RNAse contamination. Electrodes were pulled on a Sutter Instrument (Novato, CA) Model P-87 Flaming/Brown Micropipette puller, fire-polished, and filled with HBSS made with RNAse-free water. Positive pressure was applied to the pipette while navigating to the cell to minimize contamination. The electrode with an attached cell was lifted into a stream of ACSF and washed for 5 min before the cell was sucked into the pipette. Following aspiration, the contents of the electrode were ejected into a chilled, 0.5-μl, presiliconized RT tube containing a cellular mixture [1.9 μl of diethylpyrocarbonate (DEPC)-treated water, 1.0 μl of dNTP (10 mM), 0.7 μl of BSA (143 ng/μl), 0.7 μl of oligo(dT) (0.5 ug/μl), and 0.7 μl of SUPERase-in (40 U/μl)]. The mixture was stored at −80°C or used immediately for RT.

RT. The mixture was heated to 65°C and then placed on ice for ≥1 min. Single-stranded cDNA was synthesized from the cellular mRNA after 16 μl of RT Master Mix [6.0 μl of DEPC-treated water, 2.0 μl of 10× RT buffer, 4.0 μl of $MgCl_2$ (25 mM), 2.0 μl of DTT (0.1 M), 1.0 μl of RNAse Out, and 1.0 μl of Superscript III] was added. This mixture was incubated at 42°C for 50 min and then terminated by heating to 70°C for 15 min. The reactions were collected by a brief centrifugation and then incubated in 0.5 μl of RNAse H (2 U/μl) for 20 min to remove any remaining RNA from the reaction. The cDNA can be stored at −80°C or used immediately for PCR.

PCR. The single-cell cDNA generated from the RT step was subjected to conventional PCR using a programmable thermal cycler from MJ Research (Waltham, MA) and primers designed specifically to amplify the cDNA of interest (Table 1). Identification of each cDNA was based on the predicted size of each PCR product. These primers listed in Table 1 have been used successfully (4, 23). Negative controls for contamination from extraneous and genomic DNA from other sources were run for every batch of neurons. To ensure that there was no contamination from genomic DNA, reverse transcriptase was omitted. Replacing the cellular

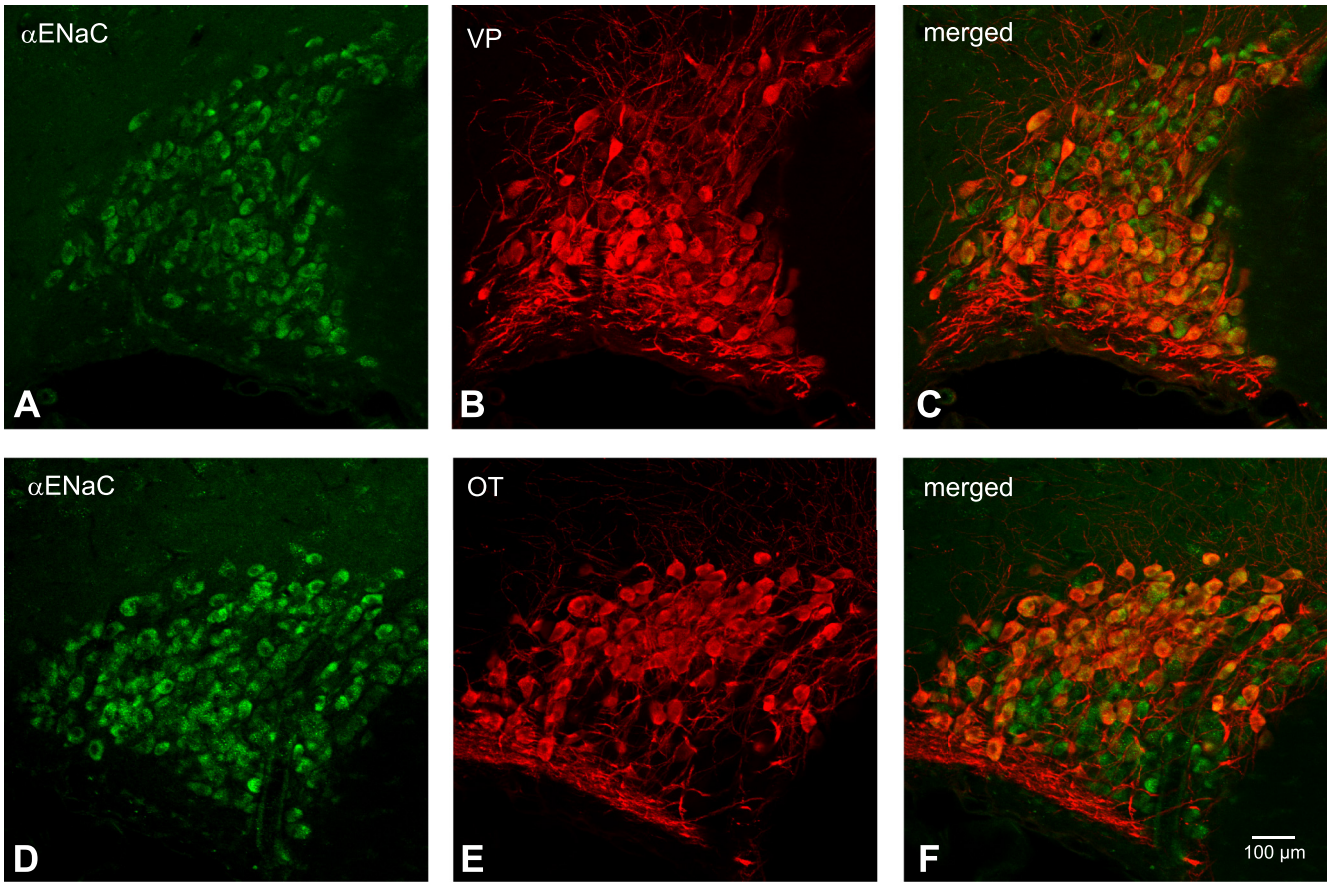

Fig. 2. Colocalization of α-epithelial Na^+ channel (ENaC) subunit with both VP-NP and OT-NP immunoreactivity in coronal section of the rat supraoptic nucleus (SON). *A* and *D*: α-ENaC subunit immunoreactivity labeled with DyLight 488-conjugated secondary antibody. Note that the intense immunoreactivity to α-ENaC subunit appeared to be confined in somata of the MNCs within the SON. *B*: VP-NP immunoreactivity labeled with DyLight 594-conjugated secondary antibody in same section and image plane as in *A*. *E*: OT-NP immunoreactivity labeled with DyLight 594-conjugated secondary antibody in same section and image plane as in *D*. *C* and *F*: the merged images revealed that α-ENaC immunoreactivity is colocalized with both VP and OT immunoreactivities within MNCs in the SON.

template with water controlled for contamination from extraneous sources.

RESULTS

Immunocytochemical Localization of ENaC Subunits in the SON and the PVN

The ENaC subunit antibodies gave consistent results in 22 animals at dilutions of 1:1,000 for α-subunits, 1:250 for β-subunits, and 1:2,000 for γ-subunits, as shown in Figs. 2–7. The most prominent immunoreactivity was observed in the SON and the PVN within coronal sections containing these nuclei. In addition, immunoreactivity was found in cuboidal epithelium of the choroid plexus and in the ventricular ependyma. Overall, the localization of α-, β-, and γ-ENaC subunits within the rat hypothalamus was similar to previous reports (3, 4). Here, we report a more detailed localization of α-, β-, and γ-ENaC within the SON and PVN performed by confocal double immunocytochemistry, using specific antibodies against ENaC subunits and antibodies against VP- or OT-NP.

An intense immunoreactivity to α-ENaC subunit was confined largely to somata of both OT and VP neurons within the SON (Fig. 2). Prominent α-ENaC immunoreactivity was also observed in somata and proximal parts of dendrites of magnocellular cells within the PVN (Fig. 3). Whereas most of these α-ENaC-immunoreactive MNCs were located in a cluster of cells in the posterior magnocellular region, α-ENaC-immunoreactive magnocellular cells were found scattered among parvocellular cells in other regions of the PVN (dorsal, medial, ventrolateral, and posterior parvocellular regions). The lateral cluster of the cells was composed mostly of VP neurons (Fig. 3, *A* and *D*); however, some OT neurons scattered around these VP neurons were immunoreactive to α-ENaC. Therefore, the α-ENaC immunoreactivity appears to be colocalized with either VP or OT MNCs. In addition to the MNCs, some parvocellular neurons that were not immunoreactive to VP- or OT-NP within dorsal, ventrolateral, and posterior parvocellular regions were also immunoreactive to α-ENaC subunit. Only sporadic α-ENaC-immunoreactive parvocellular and MNCs were observed within the medial parvocellular region of the PVN.

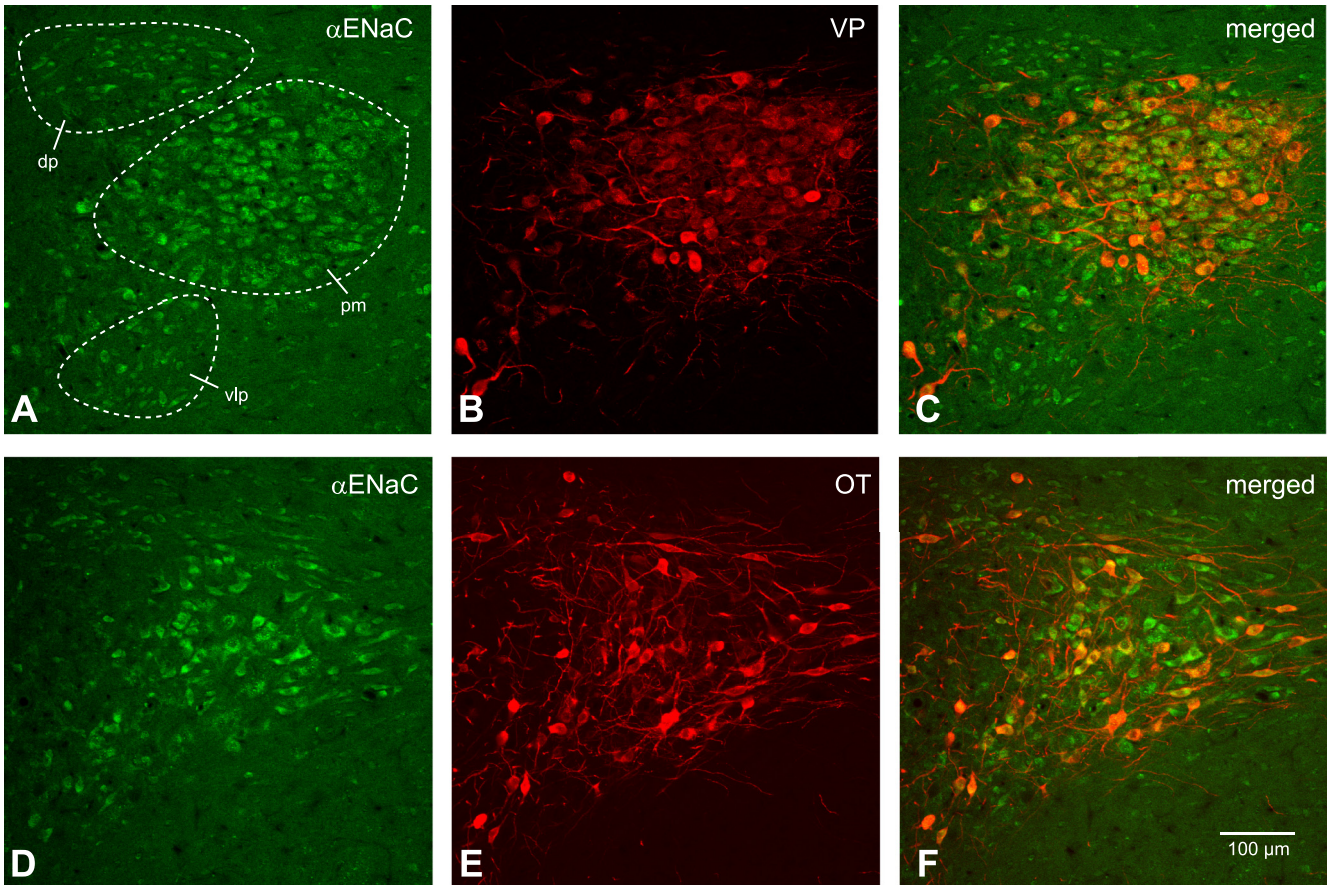

Fig. 3. Colocalization of α-ENaC subunit and VP-NP immunoreactivity in coronal section of the rat paraventricular nucleus (PVN). *A* and *D*: α-ENaC subunit immunoreactivity labeled with DyLight 488-conjugated secondary antibody. Prominent α-ENaC immunoreactivity is observed in somata and proximal parts of dendrites of MNCs within the PVN. Most of these α-ENaC-immunoreactive magnocellular cells are located in a cluster of cells in the posterior magnocellular (pm) region. The parvocellular cells in dorsal (dp), ventrolateral (vlp), and posterior parvocellular regions are also immunoreactive to α-ENaC subunit. *B*: VP-NP immunoreactivity labeled with DyLight 594-conjugated secondary antibody in same section and image plane as in *A*. Note that the VP-NP immunoreactive cells form a cluster in the lateral portion of the PVN. *E*: OT-NP immunoreactivity labeled with DyLight 594-conjugated secondary antibody in same section and image plane as in *D*. *C* and *F*: the merged images revealed that α-ENaC immunoreactivity is colocalized with both VP and OT immunoreactivities within MNCs in the PVN. Note that the lateral cluster of the cells is composed mostly of VP. MNCs are immunoreactive to α-ENaC as well as those sparsely located OT MNCs around these VP neurons. However, the parvocellular cells immunoreactive to α-ENaC within dp, vlp, and posterior parvocellular regions are not immunoreactive to VP or OT.

Immunoreactivity of β-ENaC in the SON was also confined within the somata of MNCs (Fig. 4). Although the entire area of the SON has diffuse staining that stands out from the rest of the brain area, indicating that almost all MNCs have some degree of immunoreactivity, not all of the MNCs exhibited intense somatic immunoreactivity. Double immunocytochemistry either with VP- or OT-NP revealed that these β-ENaC-immunoreactive cells were all VP and not OT neurons (Fig. 4, *C* and *F*). Not many MNCs possessed intense β-ENaC immunoreactivity in the PVN (Fig. 5); however, unlike in the SON, the immunoreactivity in these cells was not confined within the soma. Prominent immunoreactivity is seen in the dendritic processes of these neurons, located mostly in the lateral portion of the PVN. Again, double immunocytochemistry exposed that β-ENaC-immunoreactive neurons were immunoreactive to VP-NP and not OT-NP (Fig. 5, arrows). Moreover, there was no apparent β-ENaC immunoreactivity in the parvocellular cells in the PVN.

Immunoreactivity to γ-ENaC was present in many MNCs in the SON, with intense staining observed in a minority of MNCs and their sparsely distributed thick dendritic processes. (Fig. 6, arrows). Intense γ-ENaC immunoreactivity was also found in thick processes (probable dendrites) and somata of a cluster of MNCs within the posterior magnocellular portion of the PVN (Fig. 7). A more striking and consistent pattern of colocalization was present in the somata and dendrites of the MNCs within the SON (Fig. 6, *C* and *F*) and PVN (Fig. 7, *C* and *F*) after reaction with VP-NP antibody. Some γ-ENaC-immunoreactive MNCs were also immunoreactive to OT in the SON and the PVN, but only barely detectable levels of OT immunoreactivity were observed in all cases. Only weak γ-ENaC immunoreactivity was indicated in the parvocellular cells in the PVN.

An intense immunoreactivity to MR was confined largely to somata of a majority of MNCs in the SON (Fig. 8, *A* and *D*). Moreover, the MR immunoreactivity appears to be colocalized with either VP or OT MNCs in the SON (Fig. 8, *C* and *F*). In the PVN, most of prominent MR immunoreactivity was located in a cluster of MNCs in the posterior magnocellular region (Fig. 9, *A* and *D*). MR immunoreactivity was also colocalized with either VP or OT in MNCs in the PVN. In addition to the MNCs, some parvocellular neurons that were not immunoreactive to VP- or OT-NP within dorsal, ventrolateral, and posterior parvocellular regions were also immunoreactive to MR.

Single-Cell RT-PCR Detection of ENaC Subunits in the MNCs

Libraries of cDNA were derived from 12 cells dissociated from SON tissue. *Cells 1–11* had mRNA for OT-NP and/or VP-NP (Fig. 10). Unlike immunocytochemical identification

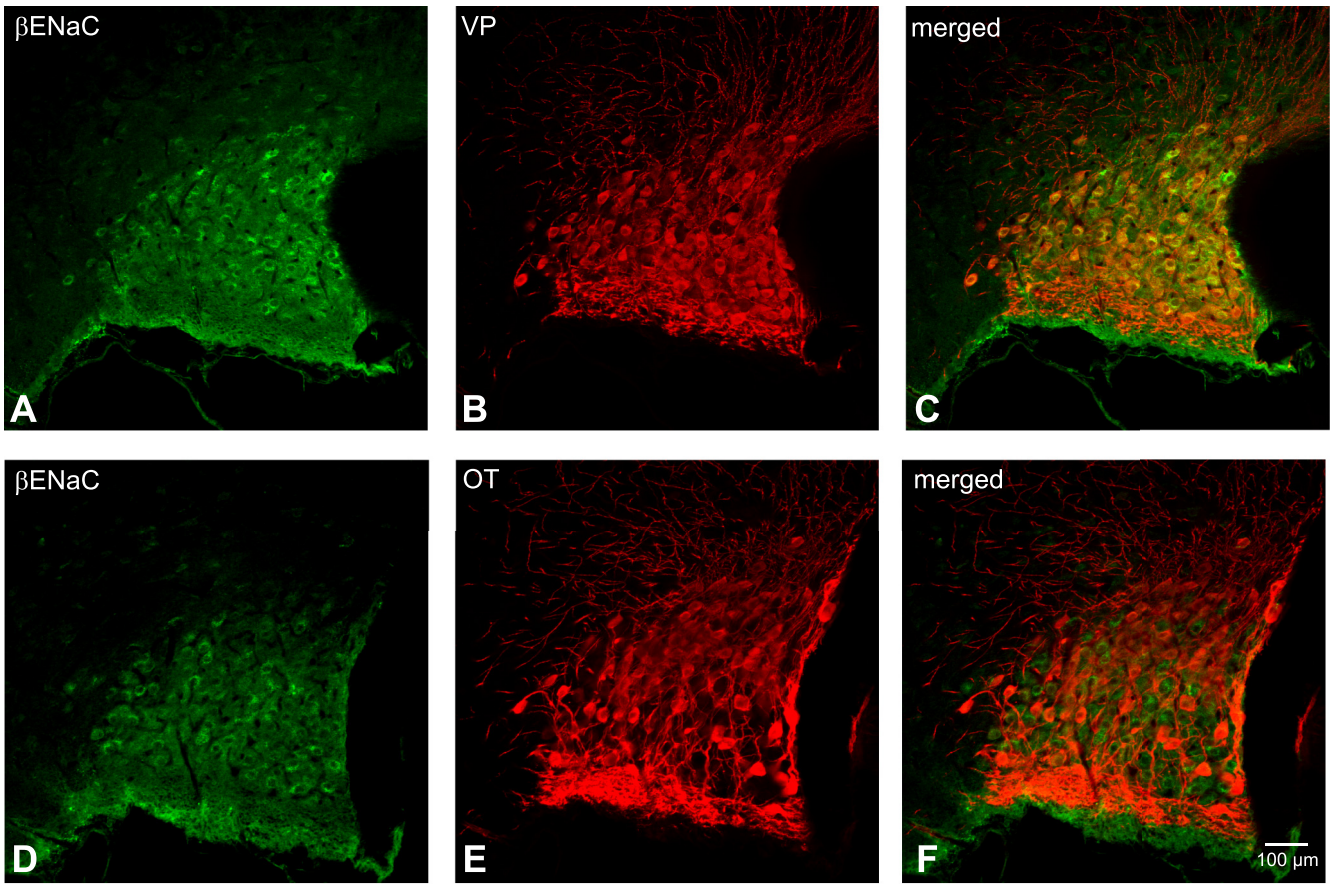

Fig. 4. Colocalization of β-ENaC subunit with both VP-NP and OT-NP immunoreactivity in coronal section of the rat SON. *A* and *D*: β-ENaC subunit immunoreactivity labeled with DyLight 488-conjugated secondary antibody. Note that immunoreactivity of β-ENaC in the SON is confined within the somata of MNCs. *B*: VP-NP immunoreactivity labeled with DyLight 594-conjugated secondary antibody in same section and image plane as in *A*. *E*: OT-NP immunoreactivity labeled with DyLight 594-conjugated secondary antibody in same section and image plane as in *D*. *C* and *F*: the merged images reveal that these β-ENaC-immunoreactive neurons are all VP and not OT immunoreactive neurons.

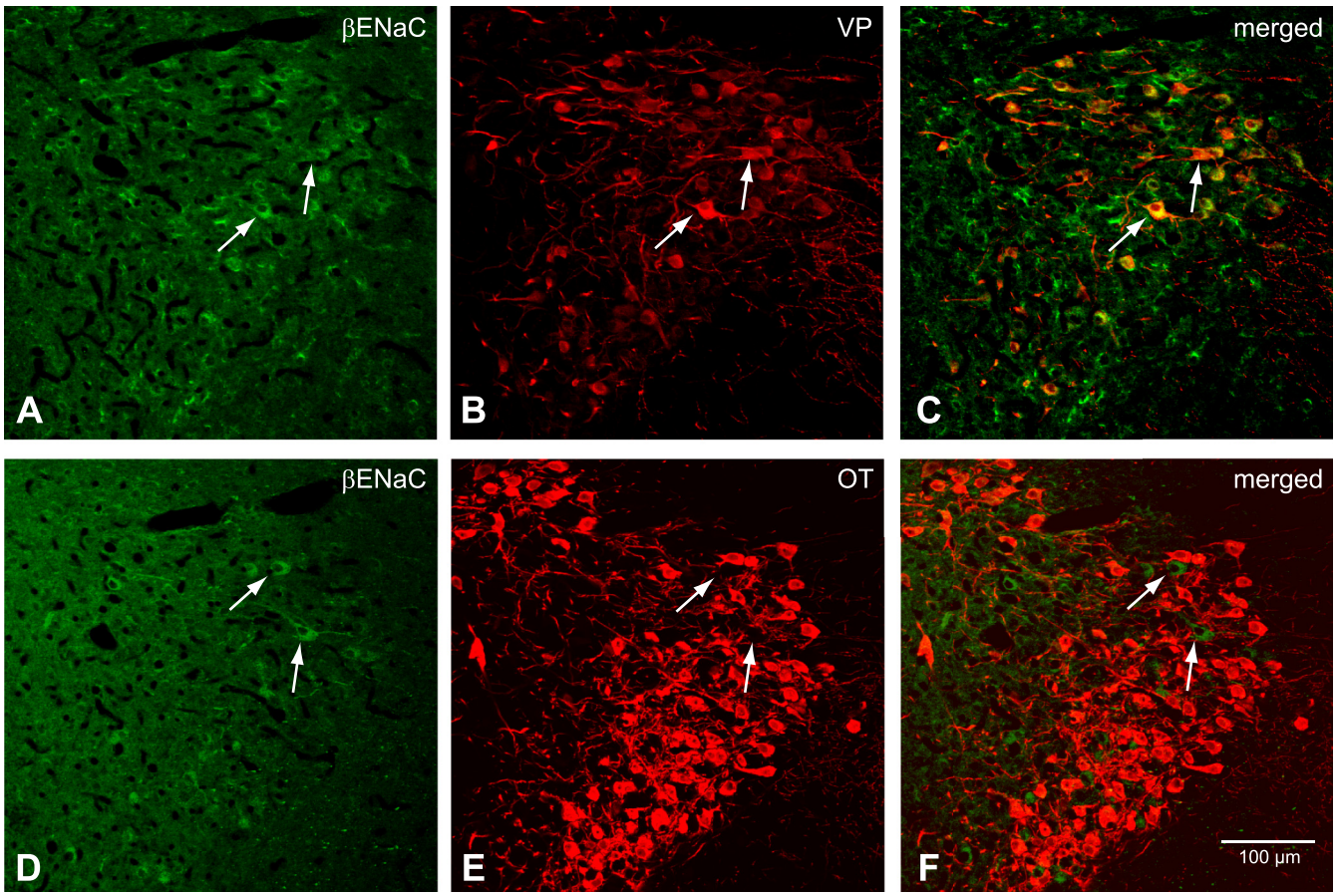

Fig. 5. Colocalization of β-ENaC subunit and VP-NP immunoreactivity in coronal section of the rat PVN. *A* and *D*: β-ENaC subunit immunoreactivity labeled with DyLight 488-conjugated secondary antibody. Note that intense immunoreactivity to β-ENaC is observed in rather scarcely distributed MNCs located mostly within the lateral portion of the PVN. However, unlike in the SON, the immunoreactivity in these cells is not confined to the soma. Prominent immunoreactivity can be seen in the dendritic processes of these neurons. There is no prominent immunoreactivity to β-ENaC observed in the parvocellular cells. *B*: VP-NP immunoreactivity labeled with DyLight 594-conjugated secondary antibody in same section and image plane as in *A*. Note that the VP-NP immunoreactive cells form a cluster in the lateral portion of the PVN. *E*: OT-NP immunoreactivity labeled with DyLight 594-conjugated secondary antibody in same section and image plane as in *D*. *C*: the merged images revealed that β-ENaC immunoreactivties appear to be colocalized only with VP within the MNCs (arrows). *F*: the merged image of *D* and *E*. Note that β-ENaC immunoreactivty is not colocalized with OT (arrows).

that demonstrates that most MNCs are phenotypically distinct, it has been well documented with single-cell RT-PCR that there is a variable amount of OT and VP mRNA coexpression in virtually all of the MNCs in the SON (23, 70, 71). Therefore, without quantitative RT-PCR it is only appropriate to state here that these dissociated cells are confirmed as MNCs producing OT or VP. Of these MNCs, mRNA for α-ENaC was found in *cells 1*, *2*, *4*, and *5*, mRNA for β-ENaC was found in *cells 1* and *3*, mRNA for γ-ENaC was found in *cells 5*, *9*, *10*, and *11*, and mRNA for MR was found in *cells 1*, *3*, *5*, *6*, *10*, and *11*. In addition, *cell 12*, although it did not contain VP or OT mRNA, contained α-ENaC, γ-ENaC, and MR. Although single-cell RT-PCR was not strong enough to obtain robust expression of each subunit in every cell, all of these mRNAs were found in a cDNA library derived from punched SON tissues. Taste receptor cells in tongue epithelia are known to express ENaC; therefore, the cDNA acquired from tongue epithelial tissue served as a positive control.

Benzamil-Sensitive Current in MNCs

To demonstrate the functional expression of ENaC, we looked for evidence of a benzamil-sensitive current in MNCs using whole cell voltage clamp. However, in the initial part of the study, a clear response to application of either amiloride or benzamil was observed only in a minority of MNCs (~7% of the recorded cell population). The majority of MNCs displayed only small changes or no change at all. This percentage was inconsistent with the number of MNCs that were immunoreactive to the antibodies against ENaC subunits. One of the possibilities for the lack of response may be an intracellular Na^+-dependent rundown observed in the cells expressing ENaC (21, 33, 60). A rise in intracellular Na^+ concentration results in a slow decrease in the current mediated by ENaC in these cells. We tried to minimize the rise in intracellular Na^+ concentration by addition of 1–2 μM amiloride in the perfusion buffer during brain slice preparation and in the incubation medium. Prior to recordings, the brain slices were transported to the chamber of the patch clamp rig that was perfused continuously with ACSF containing 1 μM benzamil. The benzamil was then washed out after establishment of stable patch clamp. In this way, robust responses to benzamil/amiloride were observed in 12 of 19 VP and 5 of 13 OT neurons.

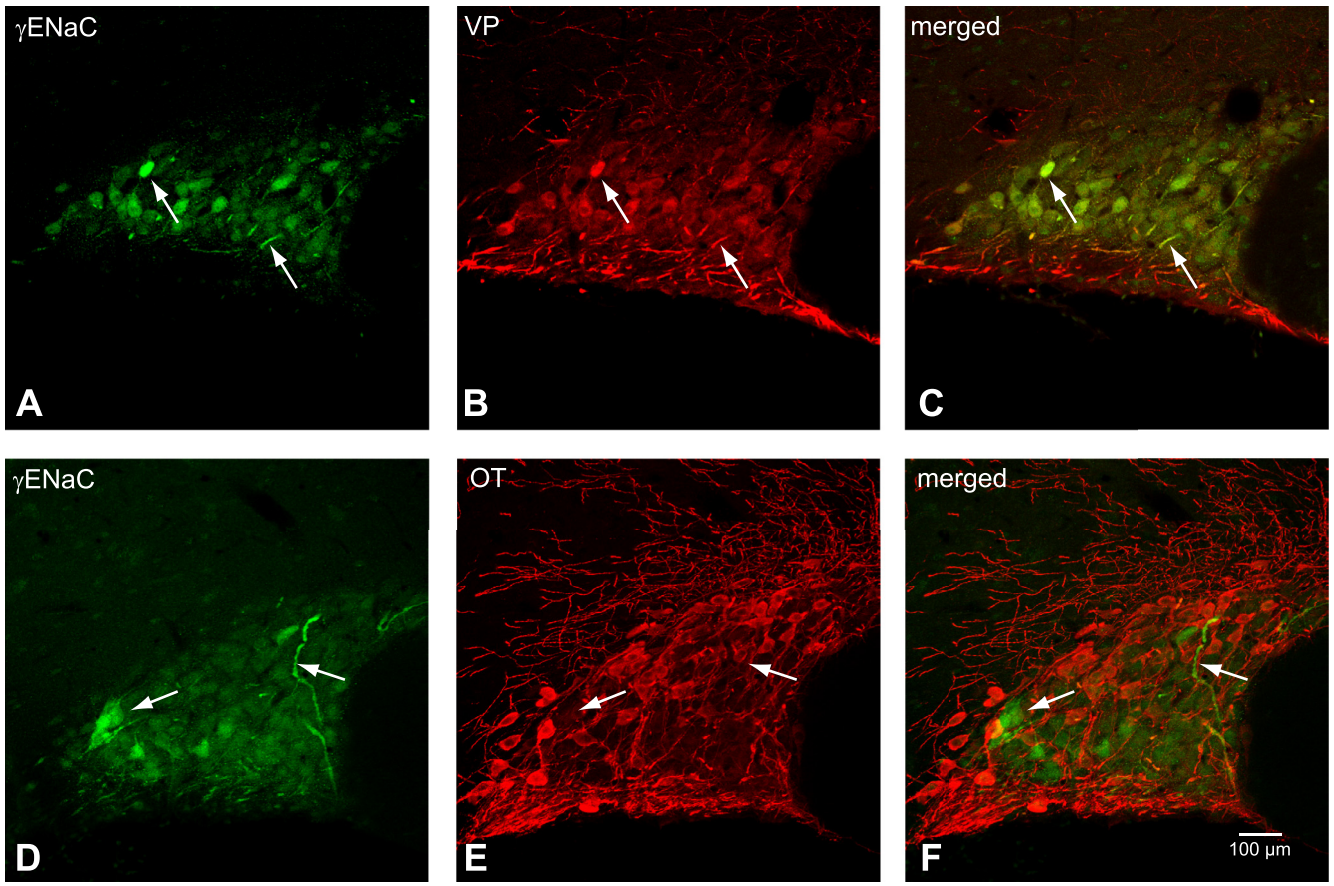

Fig. 6. Colocalization of γ-ENaC subunit and VP-NP immunoreactivity in coronal section of the rat SON. *A* and *D*: γ-ENaC subunit immunoreactivity labeled with DyLight 488-conjugated secondary antibody. Note the very intense staining observed in the minority of MNCs and their sparsely distributed thick dendritic processes (arrows), although weaker immunoreactivity appeared in many MNCs. *B*: VP-NP immunoreactivity labeled with DyLight 594-conjugated secondary antibody in same section and image plane as in *A*. *E*: OT-NP immunoreactivity labeled with DyLight 594-conjugated secondary antibody in same section and image plane as in *D*. *C* and *F*: the merged images reveal that these γ-ENaC-immunoreactive cells and dendrites are all VP and not OT immunoreactive neurons (arrows).

The steady-state current was measured while the cell was held at −70 mV in voltage clamp. Brief hyperpolarizing pulses (15 mV, 200 ms) were injected every 5 s to monitor the input resistance of the cell. Washout of amiloride from the bath resulted in an increase in a resting inward current and a decreased resistance. Subsequent bath application of the ENaC blocker benzamil (1 μM) reduced the resting inward current and decreased conductance ~1.5-fold (Fig. 9). The effect was reversed by wash of benzamil by ACSF. Figure 11 shows an example of the effect of benzamil on a VP neuron, and we observed this in six of nine VP neurons. The response was also observed in 1 of 5 OT neurons tested.

Next, we looked for the effect of benzamil on the membrane potential and the firing pattern using whole cell current clamp recording with no injected current. The removal of amiloride from the bath caused membrane depolarization, and a subsequent bath application of 1–2 μM benzamil caused membrane hyperpolarization in seven of 10 VP and four of eight OT recorded neurons. The benzamil-induced hyperpolarization was observed in both spontaneously firing and quiet cells. Figure 12 shows a VP neuron with a continuous firing pattern before application of a benzamil. One micromolar benzamil caused membrane hyperpolarization and cessation of the firing. The effect was reversed by washout of benzamil from the bath and was repeatable.

DISCUSSION

Amiloride and its analogs are known inhibitors of the degenerin/epithelial sodium channel (Deg/ENaC) superfamily of ion channels. The Deg/ENaC superfamily includes the ENaC and the acid-sensitive ion channels (ASIC) as members. ASIC1a and ASIC2a subunits were detected, and an acid- and amiloride-sensitive current was detected in SON MNCs (48). However, the concentration of amiloride required to inactivate the ASICs in the MNCs in that study was high (10–100 μM), and 1 μM amiloride had little effect on the ASIC activity. Amiloride is also a known inhibitor of several other ion transporters, including the Na^+/H^+ exchanger (NHE) and the Na^+/Ca^{++} exchanger (NCX) (36). However, amiloride at low doses is reasonably specific for ENaCs compared with the NHE and NCX (36). Nevertheless, the amiloride analog benzamil can be used to further increase selectivity for ENaC compared with the NHE or NCX. Benzamil, compared with amiloride, is ninefold more potent toward ENaCs, with markedly lower relative potency (0.08-fold) toward the NHE (14). The concentration of benzamil (1–2 μM) used in our study is

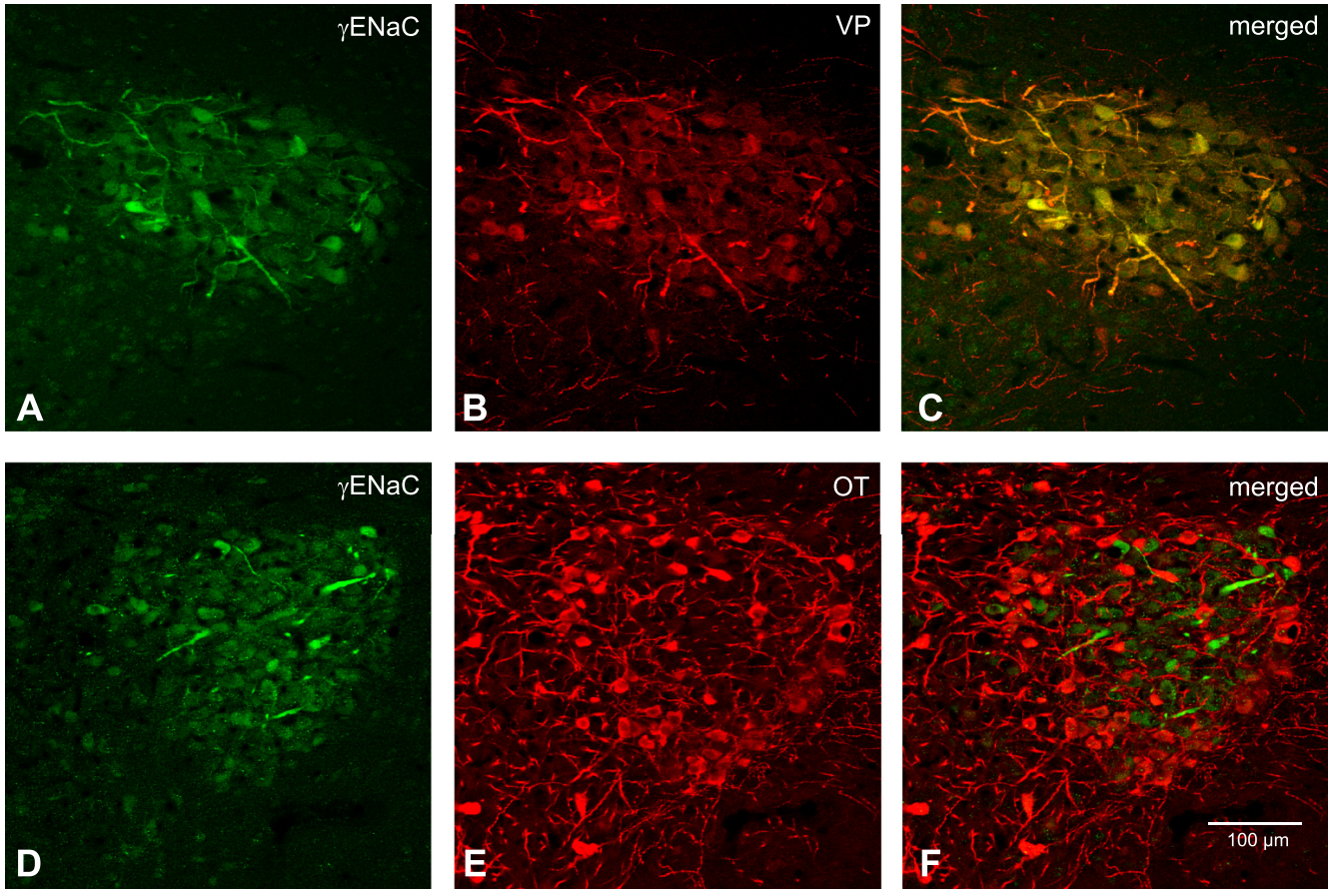

Fig. 7. Colocalization of γ-ENaC subunit with VP-NP or OT-NP immunoreactivity in coronal section of the rat PVN. *A* and *D*: γ-ENaC subunit immunoreactivity labeled with DyLight 488-conjugated secondary antibody. Note that intense immunoreactivity to γ-ENaC is observed in the MNCs and their thick processes (probable dendrites). These immunoreactive cells form a cluster in the lateral portion of the PVN. There appears to be weak immunoreactivity to γ-ENaC in the parvocellular cells. *B*: VP-NP immunoreactivity labeled with DyLight 594-conjugated secondary antibody in same section and image plane as in *A*. Note that the VP-NP immunoreactive cells form a cluster in the lateral portion of the PVN. *E*: OT-NP immunoreactivity labeled with DyLight 594-conjugated secondary antibody in same section and image plane as in *D*. *C*: the merged images revealed that γ-ENaC immunoreactivties appear to be colocalized only with VP within the MNCs located mostly in the lateral portion of the PVN. *F*: the merged image of *D* and *E*. Note that γ-ENaC immunoreactivties do not appear to be colocalized with OT.

well below the IC_{50} of benzamil for these ion exchangers. Therefore, when combined with the immunocytochemical and single-cell RT-PCR data, the electrophysiological results from this study strongly suggest the presence of functional ENaCs in the MNCs.

The release of OT and VP from the neurohypophysis depends largely on the pattern of electrical activity of their synthesizing neurons (12, 49). During the release of VP in response to hypovolemia (29), hypotension (34), and hyperosmolality (8), VP neurons increase their firing rate and adapt a phasic firing pattern comprising alternating periods of activity (7–15 Hz) and silence, each lasting tens of seconds. Plasma OT also increases in response to hypernatremia (32), and OT neurons respond to hyperosmolarity with increases in firing rate (52, 67). In the present study, the benzamil-sensitive current was identified as an inward leak current, suggesting its potential for modulating membrane potential. The activation of the benzamil-sensitive current, presumably mediated by ENaCs, would depolarize the membrane potential and allow MNCs to initiate bursting activity. Computational studies in the supraoptic MNCs showed that a Na^+ leak current is critical to the depolarizations underlying phasic firing (54). Therefore, by changes in membrane potential, the modulation of ENaCs may significantly contribute to the regulation of firing activities of these neurons and ultimately affect the release of VP and OT.

An intriguing finding in this study is that β- and γ-ENaC subunits were preferentially located in VP neurons, whereas the α-ENaC subunit was located in both VP and OT MNCs. It is generally agreed that each of the three ENaC subunits contributes to the formation of the functional channel complex (11, 19), although the actual subunit composition of the channel remains uncertain and controversial. Interestingly, α-subunits alone or with either the β- or γ-subunit can induce low but measurable amiloride-sensitive currents (11, 20). Moreover, alteration of subunit composition is suggested as a cause of the variability in single-channel properties of amiloride-sensitive ENaCs in native tissues (20). Thus, this differential subunit expression suggests that subunit composition differs between VP and OT neurons and may be physiologically important. This may be the molecular mechanism accounting for our finding that more VP (~70%) than OT neurons (~40%) were responsive to benzamil.

It is well documented that the α-subunit is regulated independently of β- and γ-subunits. Binding of aldosterone to the

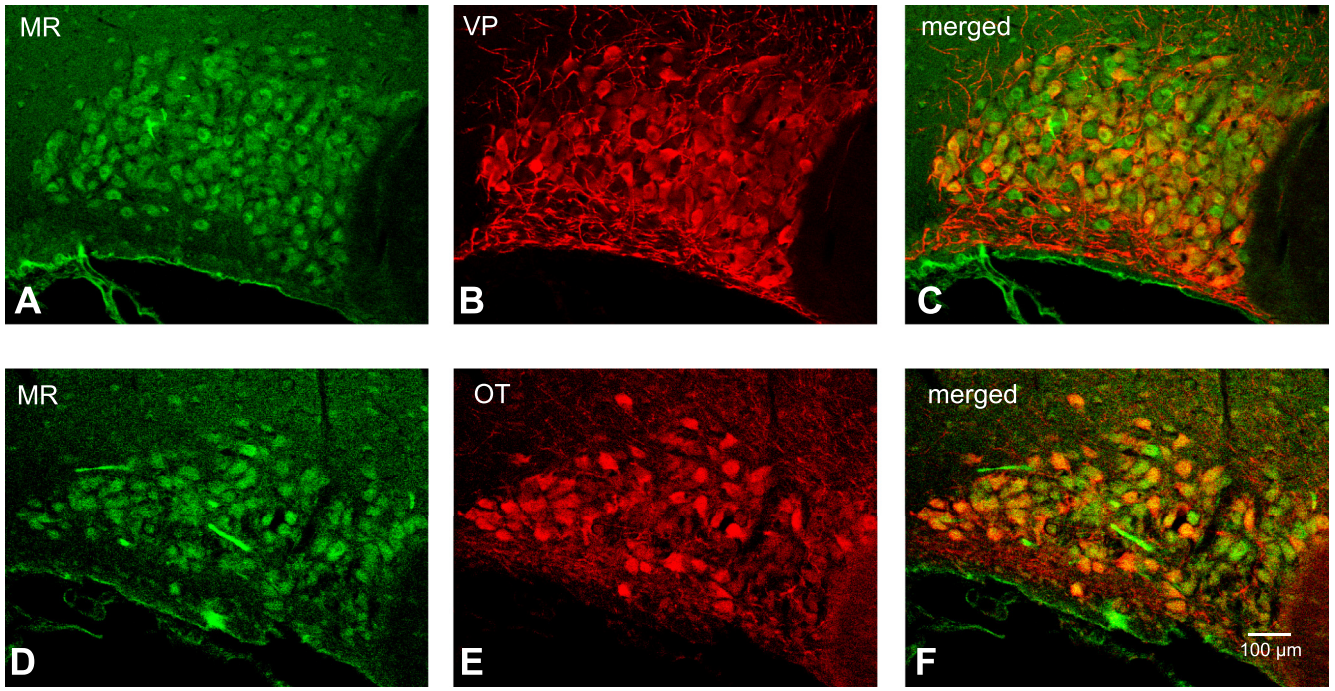

Fig. 8. Colocalization of MR with both VP-NP and OT-NP immunoreactivity in coronal section of the rat SON. *A* and *D*: MR immunoreactivity labeled with DyLight 488-conjugated secondary antibody. Note that the intense immunoreactivity to MR appeared to be confined in somata of the MNCs within the SON. *B*: VP-NP immunoreactivity labeled with DyLight 594-conjugated secondary antibody in same section and image plane as in *A*. *E*: OT-NP immunoreactivity labeled with DyLight 594-conjugated secondary antibody in same section and image plane as in *D*. *C* and *F*: the merged images revealed that MR is colocalized with both VP-NP and OT-NP immunoreactivities within MNCs in the SON (yellow).

MR was shown to predominantly increase the expression of α-subunits in rat kidney (18, 41, 42, 51, 62). Interestingly, the aldosterone regulation of ENaC subunits is somewhat tissue specific. For example, β- and γ-ENaC mRNA are selectively induced by mineralocorticoids in colon (5, 18, 51), whereas mRNA for all three subunits is primarily regulated by glucocorticoids in lung tissue (51). The presence of MR in the brain, including the SON and the PVN, was reported previously (2, 4, 28, 55). Nevertheless, the finding of MR in VP and OT MNCs in present study suggests that the expression of ENaC in the MNC is also promoted by aldosterone. Intracerebroventricular infusion of aldosterone causes hypertension Dahl-S rats, but icv infusion of a mineralocorticoid receptor antagonist prevents the salt-sensitive hypertension (25). Importantly, icv infusion of amiloride or benzamil prevents salt-induced hypertension in Dahl-S rats (26, 69). Obviously, these findings do not provide information about the upregulation of specific ENaC subunits by aldosterone in the MNCs but suggest an aldosterone-mediated activation of ENaC in these neurons.

In addition to aldosterone, VP is also known mainly to induce the expression of β- and γ-ENaC subunits in the kidney (16, 17, 46, 57). Of the three VP receptor subtypes (V_{1a}, V_{1b}, and V_2) characterized, VP appears to act through the V_2 vasopressin receptor to induce β- and γ-subunit gene expression (46). VP also stimulates translocation of preexisting intracellular pools of ENaC subunits to the apical membrane of the principal cells in the collecting duct, promoting Na^+ reabsorption in kidney (58). VP neurons not only secrete VP at the nerve terminals in the neurohypophysis but also release VP in the extracellular space of the SON and PVN from their soma and dendrites (37, 39, 45). A recent study demonstrated that the V_2-like receptor mediates the ability of somatodendritically released VP to facilitate cell volume regulation in VP neurons (56). In addition, somato-dendritic release of VP is known to modulate electrical activity of VP neurons primarily via the V_{1a} receptor (15, 40, 43, 44). Nevertheless, the presence of V_2-like receptors on VP neurons implies the possibility that the β- and γ-subunits in VP neurons could be regulated by somatodendritic release of VP by mechanisms similar to their regulation in the nephron.

Another finding of interest in the current study is the presence of α-ENaC immunoreactivity in a subpopulation of the parvocellular neurons in the dorsal and ventrolateral parvocellular regions of the PVN. These PVN parvocellular neurons were not immunoreactive for OT-NP or VP-NP and were found in regions that send projections to either the rostral ventrolateral medulla that contain sympathetic premotor neurons or the spinal sympathetic preganglionic neurons to affect the autonomic nervous system (30, 50, 61). In addition, there was no clear immunoreactivity for β- and γ-subunits in these parvocellular populations. This solitary expression of α-ENaC in the parvocellular cell population suggests a different role for ENaCs in these neurons compared with MNCs. A recent study using c-Fos immunoreactivity to assess the role of benzamil-sensitive proteins in the brain following chronic DOCA salt treatment showed that icv benzamil treatment decreased c-Fos immunoreactivity in the SON and in medial parvocellular and posterior magnocellular neurons of the PVN but not areas associated with regulation of sympathetic activity (1). Thus, these authors suggested that icv benzamil attenuates DOCA salt hypertension by modulation of neuroendocrine-related nuclei rather than inhibition of sympathetic premotor neurons

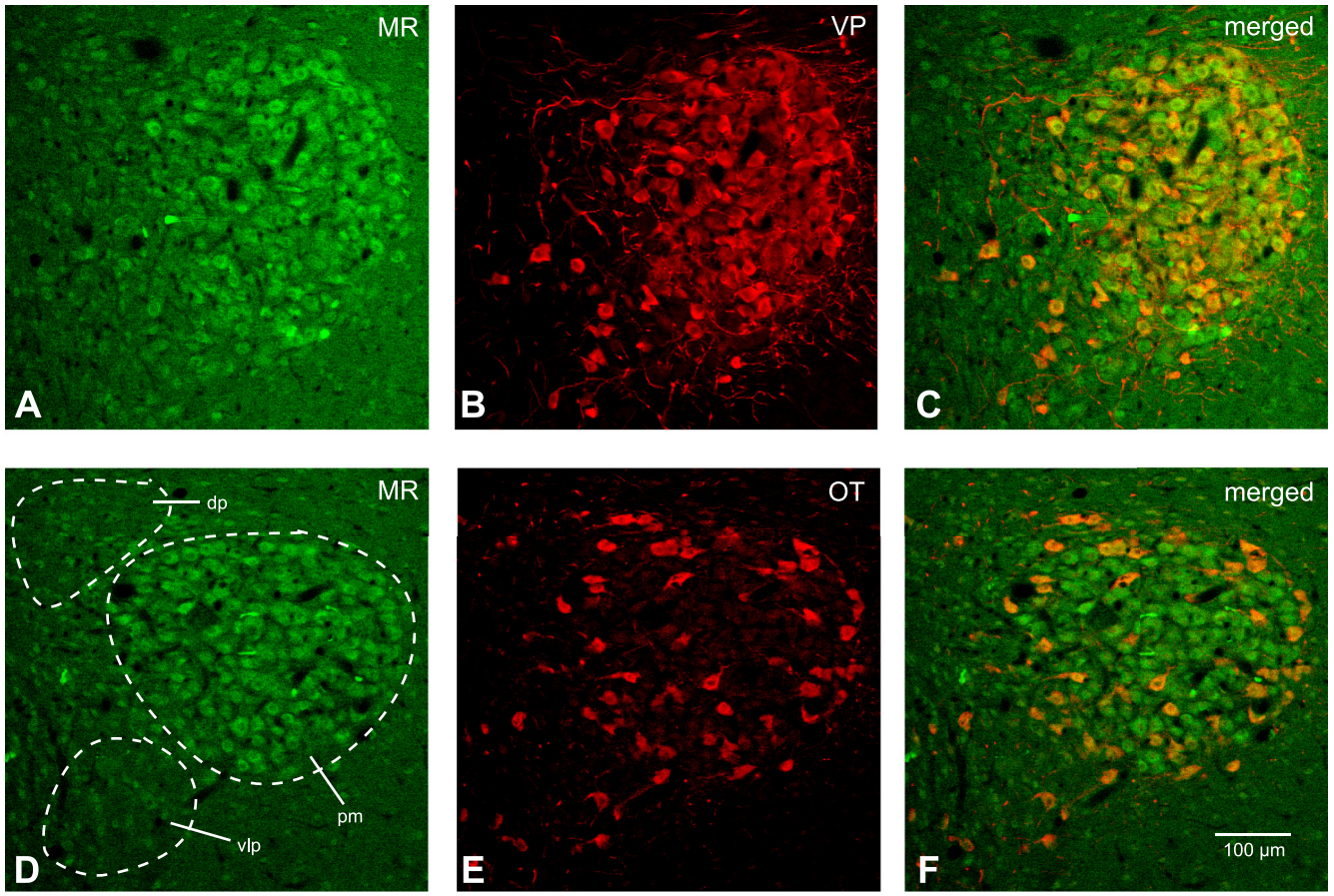

Fig. 9. Colocalization of MR with VP-NP or OT-NP immunoreactivity in coronal section of the rat SON. *A* and *D*: MR immunoreactivity labeled with DyLight 488-conjugated secondary antibody. Prominent MR immunoreactivity is observed in somata of MNCs within the PVN. Most of these MR-immunoreactive MNCs are located in a cluster of cells in the posterior magnocellular region (pm). Considerable MR immunoreactivity was also observed in the parvocellular cells in dp, vlp, and posterior parvocellular regions. *B*: VP-NP immunoreactivity labeled with DyLight 594-conjugated secondary antibody in same section and image plane as in *A*. Note that the VP-NP immunoreactive cells form a cluster in the lateral portion of the PVN. *E*: OT-NP immunoreactivity labeled with DyLight 594-conjugated secondary antibody in same section and image plane as in *D*. *C* and *F*: the merged images revealed that MR immunoreactivity is colocalized (yellow) with both VP-NP and OT-NP immunoreactivities within MNCs in the PVN. Note that the lateral cluster of the cells is composed mostly of VP MNCs that are immunoreactive to MR as well as some sparsely located OT MNCs around these VP neurons. However, the parvocellular cells immunoreactive to MR within dp, vlp, and posterior parvocellular regions are not immunoreactive to VP or OT.

in the PVN. These findings, along with the report that α-subunits alone can carry low but measurable amiloride-sensitive currents (11, 20), suggest the ENaCs in these nonneuroendocrine parvocellular cells may have different biophysical characteristics from those in the MNCs.

In taste receptor cells, ENaCs act as Na^+ sensors and play an important role in salt taste transduction (22, 35, 38). The existence of neuronal elements that are sensitive to Na^+ was suggested, since the effects induced by icv administration of hypertonic NaCl were shown to originate from the changes in CSF Na^+ concentration but not in CSF osmolarity (9, 10). Therefore, it is possible that ENaCs in MNCs also act as Na^+ sensors, where they could underlie the specific Na^+ sensitivity attributed previously to MNCs in the SON (66).

ACKNOWLEDGMENTS

We thank Drs. J. T. Caprio and E. L. Gleason for reading earlier versions of this manuscript, Dr. M. A. Knepper for providing ENaC antibodies, and Grant Bertolet for technical assistance.

GRANTS

This work was supported by National Institutes of Health Grants R21-HL-0932728 (R. Teruyama), R21-HL-0932728S (R. Teruyama), R01-NS-2394-19 (W. E. Armstrong), R01-NS23941-19S (W. E. Armstrong), and R56-NS-23941-20 (W. E. Armstrong) and in part from a grant to the Louisiana State University College of Science from the Howard Hughes Medical Institute Biomedical Education Program.

DISCLOSURES

The authors have nothing to disclose.

AUTHOR CONTRIBUTIONS

R.T. did the conception and design of the research; R.T., M.S., L.L.W., and N.E.W. performed the experiments; R.T. and M.S. analyzed the data; R.T. interpreted the results of the experiments; R.T., L.L.W., and N.E.W. prepared the figures; R.T. drafted the manuscript; R.T. and W.E.A. edited and revised the manuscript; R.T. approved the final version of the manuscript.

REFERENCES

1. **Abrams JM, Engeland WC, Osborn JW.** Effect of intracerebroventricular benzamil on cardiovascular and central autonomic responses to DOCA-salt treatment. *Am J Physiol Regul Integr Comp Physiol* 299: R1500–R1510, 2010.
2. **Ahima R, Krozowski Z, Harlan R.** Type I corticosteroid receptor-like immunoreactivity in the rat CNS: distribution and regulation by corticosteroids. *J Comp Neurol* 313: 522–538, 1991.

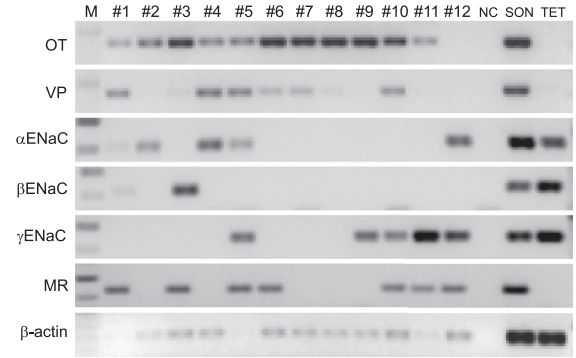

Fig. 10. Single-cell RT-PCR to detect transcripts in individual dissociated MNCs. Libraries of cDNA were derived from 12 cells dissociated from SON tissue. *Cells 1–11* had mRNA for OT and/or VP, confirming that they were MNCs. Of these MNCs, α-ENaC mRNA was found in *cells 1*, *2*, *4*, and *5*, β-ENaC mRNA was found in *cells 1* and *3*, γ-ENaC mRNA was found in *cells 5*, *9*, *10*, and *11*, and mRNA for MR was found in *cells 1*, *3*, *5*, *6*, *10*, and *11*. In addition, *cell 12*, although it did not contain VP or OT mRNA, contained α-ENaC, γ-ENaC, and MR. All of these mRNAs were found in cDNA library derived from punched SON tissues. Taste receptor cells in tongue epithelia are known to express ENaC, and therefore, the cDNA acquired from tongue epithelial tissue (TET) served as a positive control. Negative controls (NC) for contamination from extraneous and genomic DNA from other sources were run for every batch of neurons. Amplifications with no cDNA yielded negative results.

3. **Amin MS, Reza E, Wang H, Leenen FH.** Sodium transport in the choroid plexus and salt-sensitive hypertension. *Hypertension* 54: 860–867, 2009.
4. **Amin MS, Wang HW, Reza E, Whitman SC, Tuana BS, Leenen FH.** Distribution of epithelial sodium channels and mineralocorticoid receptors in cardiovascular regulatory centers in rat brain. *Am J Physiol Regul Integr Comp Physiol* 289: R1787–R1797, 2005.
5. **Asher C, Wald H, Rossier BC, Garty H.** Aldosterone-induced increase in the abundance of Na^+ channel subunits. *Am J Physiol Cell Physiol* 271: C605–C611, 1996.
6. **Ben-Barak Y, Russell JT, Whitnall MH, Ozato K, Gainer H.** Neurophysin in the hypothalamo-neurohypophysial system. I. Production and characterization of monoclonal antibodies. *J Neurosci* 5: 81–97, 1985.
7. **Benos DJ, Awayda MS, Ismailov II, Johnson JP.** Structure and function of amiloride-sensitive Na^+ channels. *J Membr Biol* 143: 1–18, 1995.
8. **Brimble MJ, Dyball RE.** Characterization of the responses of oxytocin- and vasopressin-secreting neurones in the supraoptic nucleus to osmotic stimulation. *J Physiol* 271: 253–271, 1977.
9. **Bunag RD, Miyajima E.** Baroreflex impairment precedes hypertension during chronic cerebroventricular infusion of hypertonic sodium chloride in rats. *J Clin Invest* 74: 2065–2073, 1984.
10. **Bunag RD, Miyajima E.** Sympathetic hyperactivity elevates blood pressure during acute cerebroventricular infusions of hypertonic salt in rats. *J Cardiovasc Pharmacol* 6: 844–851, 1984.
11. **Canessa CM, Schild L, Buell G, Thorens B, Gautschi I, Horisberger JD, Rossier BC.** Amiloride-sensitive epithelial Na^+ channel is made of three homologous subunits. *Nature* 367: 463–467, 1994.
12. **Cazalis M, Dayanithi G, Nordmann JJ.** The role of patterned burst and interburst interval on the excitation-coupling mechanism in the isolated rat neural lobe. *J Physiol* 369: 45–60, 1985.
13. **Conrad KP, Gellai M, North WG, Valtin H.** Influence of oxytocin on renal hemodynamics and electrolyte and water excretion. *Am J Physiol Renal Fluid Electrolyte Physiol* 251: F290–F296, 1986.
14. **Cuthbert AW, Fanelli GM.** Effects of some pyrazinecarboxamides on sodium transport in frog skin. *Br J Pharmacol* 63: 139–149, 1978.
15. **Dayanithi G, Widmer H, Richard P.** Vasopressin-induced intracellular Ca^{2+} increase in isolated rat supraoptic cells. *J Physiol* 490: 713–727, 1996.
16. **Djelidi S, Fay M, Cluzeaud F, Escoubet B, Eugene E, Capurro C, Bonvalet JP, Farman N, Blot-Chabaud M.** Transcriptional regulation of sodium transport by vasopressin in renal cells. *J Biol Chem* 272: 32919–32924, 1997.
17. **Ecelbarger CA, Kim GH, Terris J, Masilamani S, Mitchell C, Reyes I, Verbalis JG, Knepper MA.** Vasopressin-mediated regulation of epithelial sodium channel abundance in rat kidney. *Am J Physiol Renal Physiol* 279: F46–F53, 2000.
18. **Escoubet B, Coureau C, Bonvalet JP, Farman N.** Noncoordinate regulation of epithelial Na channel and Na pump subunit mRNAs in kidney and colon by aldosterone. *Am J Physiol Cell Physiol* 272: C1482–C1491, 1997.
19. **Firsov D, Gautschi I, Merillat AM, Rossier BC, Schild L.** The heterotetrameric architecture of the epithelial sodium channel (ENaC). *EMBO J* 17: 344–352, 1998.
20. **Fyfe GK, Canessa CM.** Subunit composition determines the single channel kinetics of the epithelial sodium channel. *J Gen Physiol* 112: 423–432, 1998.
21. **Garty H, Palmer LG.** Epithelial sodium channels: function, structure, and regulation. *Physiol Rev* 77: 359–396, 1997.
22. **Gilbertson TA, Kinnamon SC.** Making sense of chemicals. *Chem Biol* 3: 233–237, 1996.
23. **Glasgow E, Kusano K, Chin H, Mezey E, Young WS 3rd, Gainer H.** Single cell reverse transcription-polymerase chain reaction analysis of rat supraoptic magnocellular neurons: neuropeptide phenotypes and high voltage-gated calcium channel subtypes. *Endocrinology* 140: 5391–5401, 1999.
24. **Gomez-Sanchez CE, de Rodriguez AF, Romero DG, Estess J, Warden MP, Gomez-Sanchez MT, Gomez-Sanchez EP.** Development of a panel of monoclonal antibodies against the mineralocorticoid receptor. *Endocrinology* 147: 1343–1348, 2006.
25. **Gomez-Sanchez EP, Fort C, Thwaites D.** Central mineralocorticoid receptor antagonism blocks hypertension in Dahl S/JR rats. *Am J Physiol Endocrinol Metab* 262: E96–E99, 1992.
26. **Gomez-Sanchez EP, Gomez-Sanchez CE.** Effect of central amiloride infusion on mineralocorticoid hypertension. *Am J Physiol Endocrinol Metab* 267: E754–E758, 1994.
27. **Gomez-Sanchez EP, Gomez-Sanchez CE.** Effect of central infusion of benzamil on Dahl S rat hypertension. *Am J Physiol Heart Circ Physiol* 269: H1044–H1047, 1995.
28. **Han F, Ozawa H, Matsuda K, Nishi M, Kawata M.** Colocalization of mineralocorticoid receptor and glucocorticoid receptor in the hippocampus and hypothalamus. *Neurosci Res* 51: 371–381, 2005.

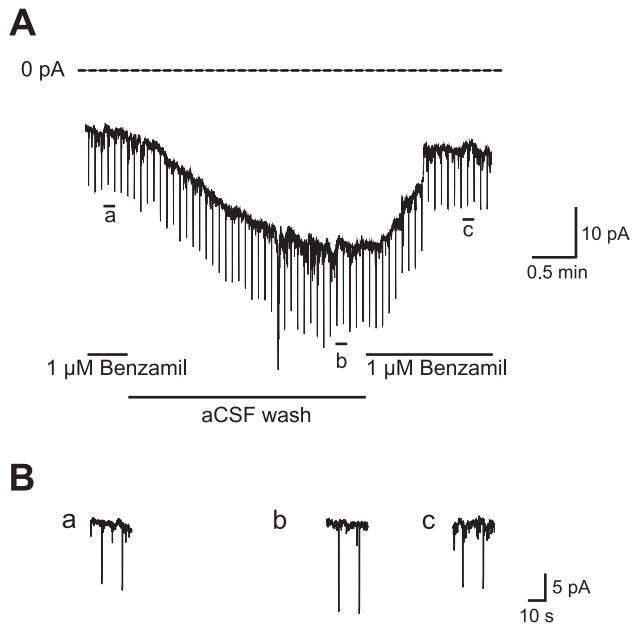

Fig. 11. A representative recording from a VP neuron showing the effect of benzamil on the current measured at −70 mV. The steady-state current was measured when the cell was held at −70 mV in voltage clamp. Brief hyperpolarizing pulses (200 ms, −15 mV) were injected every 5 s to monitor the input resistance of the cell. Washing amiloride from the bath resulted in an increase in a resting inward current and a decreased resistance. Subsequent bath application of ENaC blocker benzamil (1 μM) reduced the resting inward current and decreased conductance ~1.5-fold. The effect was reversed by wash of benzamil by artificial cerebrospinal fluid (ACSF).

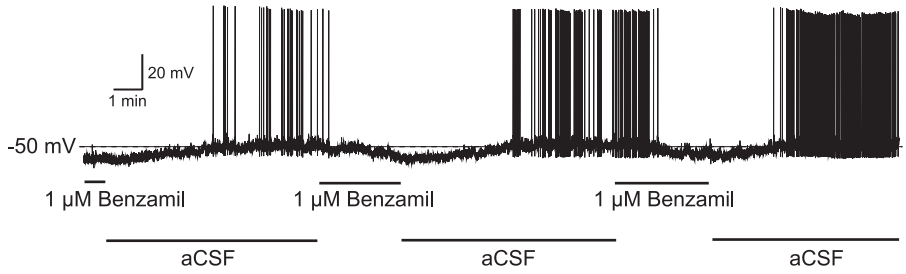

Fig. 12. An example of the effect of benzamil on the membrane potential and the firing pattern of VP neuron. The removal of benzamil from the bath caused depolarization and firing of the VP cell. Subsequent bath application of 1 μM benzamil caused membrane hyperpolarization and cessation of the firing. No current was injected during the recording.

29. **Harris MC, Dreifuss JJ, Legros JJ.** Excitation of phasically firing supraoptic neurones during vasopressin release. *Nature* 258: 80–82, 1975.
30. **Hosoya Y, Sugiura Y, Okado N, Loewy AD, Kohno K.** Descending input from the hypothalamic paraventricular nucleus to sympathetic preganglionic neurons in the rat. *Exp Brain Res* 85: 10–20, 1991.
31. **Huang W, Lee SL, Sjoquist M.** Effects of neurohypophyseal antagonists in postnephrectomy natriuresis in male rats. *Kidney Int* 45: 692–699, 1994.
32. **Huang W, Lee SL, Sjoquist M.** Natriuretic role of endogenous oxytocin in male rats infused with hypertonic NaCl. *Am J Physiol Regul Integr Comp Physiol* 268: R634–R640, 1995.
33. **Kellenberger S, Gautschi I, Rossier BC, Schild L.** Mutations causing Liddle syndrome reduce sodium-dependent downregulation of the epithelial sodium channel in the Xenopus oocyte expression system. *J Clin Invest* 101: 2741–2750, 1998.
34. **Khanna S, Sibbald JR, Smith DW, Day TA.** Initiation of rat vasopressin cell responses to simulated hypotensive hemorrhage. *Am J Physiol Regul Integr Comp Physiol* 267: R1142–R1149, 1994.
35. **Kinnamon SC, Margolskee RF.** Mechanisms of taste transduction. *Curr Opin Neurobiol* 6: 506–513, 1996.
36. **Kleyman TR, Cragoe EJ Jr.** Amiloride and its analogs as tools in the study of ion transport. *J Membr Biol* 105: 1–21, 1988.
37. **Landgraf R, Ludwig M.** Vasopressin release within the supraoptic and paraventricular nuclei of the rat brain: osmotic stimulation via microdialysis. *Brain Res* 558: 191–196, 1991.
38. **Lindemann B.** Taste reception. *Physiol Rev* 76: 718–766, 1996.
39. **Ludwig M.** Dendritic release of vasopressin and oxytocin. *J Neuroendocrinol* 10: 881–895, 1998.
40. **Ludwig M, Leng G.** Autoinhibition of supraoptic nucleus vasopressin neurons in vivo: a combined retrodialysis/electrophysiological study in rats. *Eur J Neurosci* 9: 2532–2540, 1997.
41. **MacDonald P, MacKenzie S, Ramage LE, Seckl JR, Brown RW.** Corticosteroid regulation of amiloride-sensitive sodium-channel subunit mRNA expression in mouse kidney. *J Endocrinol* 165: 25–37, 2000.
42. **Masilamani S, Kim GH, Mitchell C, Wade JB, Knepper MA.** Aldosterone-mediated regulation of ENaC alpha, beta, and gamma subunit proteins in rat kidney. *J Clin Invest* 104: R19–R23, 1999.
43. **Moos F, Gouzenes L, Brown D, Dayanithi G, Sabatier N, Boissin L, Rabie A, Richard P.** New aspects of firing pattern autocontrol in oxytocin and vasopressin neurones. *Adv Exp Med Biol* 449: 153–162, 1998.
44. **Moos FC, Ingram CD.** Electrical recordings of magnocellular supraoptic and paraventricular neurons displaying both oxytocin- and vasopressin-related activity. *Brain Res* 669: 309–314, 1995.
45. **Neumann I, Russell JA, Landgraf R.** Oxytocin and vasopressin release within the supraoptic and paraventricular nuclei of pregnant, parturient and lactating rats: a microdialysis study. *Neuroscience* 53: 65–75, 1993.
46. **Nicco C, Wittner M, DiStefano A, Jounier S, Bankir L, Bouby N.** Chronic exposure to vasopressin upregulates ENaC and sodium transport in the rat renal collecting duct and lung. *Hypertension* 38: 1143–1149, 2001.
47. **Nishimura M, Ohtsuka K, Nanbu A, Takahashi H, Yoshimura M.** Benzamil blockade of brain Na^+ channels averts Na^+-induced hypertension in rats. *Am J Physiol Regul Integr Comp Physiol* 274: R635–R644, 1998.
48. **Ohbuchi T, Sato K, Suzuki H, Okada Y, Dayanithi G, Murphy D, Ueta Y.** Acid-sensing ion channels in rat hypothalamic vasopressin neurons of the supraoptic nucleus. *J Physiol* 588: 2147–2162, 2010.
49. **Poulain DA, Wakerley JB.** Electrophysiology of hypothalamic magnocellular neurones secreting oxytocin and vasopressin. *Neuroscience* 7: 773–808, 1982.
50. **Ranson RN, Motawei K, Pyner S, Coote JH.** The paraventricular nucleus of the hypothalamus sends efferents to the spinal cord of the rat that closely appose sympathetic preganglionic neurones projecting to the stellate ganglion. *Exp Brain Res* 120: 164–172, 1998.
51. **Renard S, Voilley N, Bassilana F, Lazdunski M, Barbry P.** Localization and regulation by steroids of the alpha, beta and gamma subunits of the amiloride-sensitive Na^+ channel in colon, lung and kidney. *Pflugers Arch* 430: 299–307, 1995.
52. **Renaud LP, Bourque CW.** Neurophysiology and neuropharmacology of hypothalamic magnocellular neurons secreting vasopressin and oxytocin. *Prog Neurobiol* 36: 131–169, 1991.
53. **Roberts MM, Robinson AG, Fitzsimmons MD, Grant F, Lee WS, Hoffman GE.** c-fos expression in vasopressin and oxytocin neurons reveals functional heterogeneity within magnocellular neurons. *Neuroendocrinology* 57: 388–400, 1993.
54. **Roper P, Callaway J, Shevchenko T, Teruyama R, Armstrong W.** AHP's, HAP's and DAP's: how potassium currents regulate the excitability of rat supraoptic neurones. *J Comput Neurosci* 15: 367–389, 2003.
55. **Sanchez MM, Young LJ, Plotsky PM, Insel TR.** Distribution of corticosteroid receptors in the rhesus brain: relative absence of glucocorticoid receptors in the hippocampal formation. *J Neurosci* 20: 4657–4668, 2000.
56. **Sato K, Numata T, Saito T, Ueta Y, Okada Y.** V_2 receptor-mediated autocrine role of somatodendritic release of AVP in rat vasopressin neurons under hypo-osmotic conditions. *Sci Signal* 4: ra5, 2011.
57. **Sauter D, Fernandes S, Goncalves-Mendes N, Boulkroun S, Bankir L, Loffing J, Bouby N.** Long-term effects of vasopressin on the subcellular localization of ENaC in the renal collecting system. *Kidney Int* 69: 1024–1032, 2006.
58. **Schafer JA, Hawk CT.** Regulation of Na^+ channels in the cortical collecting duct by AVP and mineralocorticoids. *Kidney Int* 41: 255–268, 1992.
59. **Sladek CD.** Antidiuretic hormone: synthesis and release. In: *Handbook of Physiology*, edited by Fray JCS. New York: Oxford University Press, 2000, sect. 7, p. 436–495.
60. **Staub O, Abriel H, Plant P, Ishikawa T, Kanelis V, Saleki R, Horisberger JD, Schild L, Rotin D.** Regulation of the epithelial Na^+ channel by Nedd4 and ubiquitination. *Kidney Int* 57: 809–815, 2000.
61. **Stocker SD, Cunningham JT, Toney GM.** Water deprivation increases Fos immunoreactivity in PVN autonomic neurons with projections to the spinal cord and rostral ventrolateral medulla. *Am J Physiol Regul Integr Comp Physiol* 287: R1172–R1183, 2004.
62. **Stokes JB, Sigmund RD.** Regulation of rENaC mRNA by dietary NaCl and steroids: organ, tissue, and steroid heterogeneity. *Am J Physiol Cell Physiol* 274: C1699–C1707, 1998.
63. **Teiwes J, Toto RD.** Epithelial sodium channel inhibition in cardiovascular disease. A potential role for amiloride. *Am J Hypertens* 20: 109–117, 2007.
64. **Teruyama R, Armstrong WE.** Calcium-dependent fast depolarizing afterpotentials in vasopressin neurons in the rat supraoptic nucleus. *J Neurophysiol* 98: 2612–2621, 2007.
65. **Teruyama R, Armstrong WE.** Enhancement of calcium-dependent afterpotentials in oxytocin neurons of the rat supraoptic nucleus during lactation. *J Physiol* 566: 505–518, 2005.
66. **Voisin DL, Bourque CW.** Integration of sodium and osmosensory signals in vasopressin neurons. *Trends Neurosci* 25: 199–205, 2002.

67. **Wakerley JB, ter Haar MB.** Plasma concentrations of prolactin and thyrotrophin during suckling: effects of stimulation of the median eminence. *J Endocrinol* 76: 557–558, 1978.
68. **Wang H, Leenen FH.** Brain sodium channels and central sodium-induced increases in brain ouabain-like compound and blood pressure. *J Hypertens* 21: 1519–1524, 2003.
69. **Wang H, Leenen FH.** Brain sodium channels mediate increases in brain "ouabain" and blood pressure in Dahl S rats. *Hypertension* 40: 96–100, 2002.
70. **Xi D, Kusano K, Gainer H.** Quantitative analysis of oxytocin and vasopressin messenger ribonucleic acids in single magnocellular neurons isolated from supraoptic nucleus of rat hypothalamus. *Endocrinology* 140: 4677–4682, 1999.
71. **Yamashita M, Glasgow E, Zhang BJ, Kusano K, Gainer H.** Identification of cell-specific messenger ribonucleic acids in oxytocinergic and vasopressinergic magnocellular neurons in rat supraoptic nucleus by single-cell differential hybridization. *Endocrinology* 143: 4464–4476, 2002.